RESEARCH ARTICLE

Editorial Process: Submission:05/12/2025 Acceptance:14/09/2026 Published:27/09/2026

In Silico Study of Micheliolide Derivatives as Potential Non-Small Cell Lung Cancer Drugs Targeting the Epidermal Growth Factor Receptor

Sahat Halim[1,2]*, Aziza Harris[2], Steffi Cong Andi Nata[2], Achmad Mudassir Muchlis[2], Darmadi[1], Herikurniawan[2], Cleopas Martin Rumende[2]

Abstract

Objective: To identify Micheliolide-based derivatives with favorable drug-like properties and inhibitory potential against the epidermal growth factor receptor (*EGFR*) using an integrated in silico approach. **Methods:** Micheliolide derivatives were evaluated for pharmacokinetic and toxicity profiles using SwissADME and ADMET-AI, and anticancer-related activity was predicted using PASS Online. Molecular docking was performed with AutoDock Vina using erlotinib as a reference ligand. The top-ranked compounds were further examined through 50 ns molecular dynamics simulations to assess complex stability. **Results:** All derivatives fulfilled Lipinski's criteria. Several compounds demonstrated favorable predicted bioavailability and anticancer probability. Docking analysis identified compound 10 as having the strongest binding affinity, followed by compounds 19 and 3, with all three occupying the same *EGFR* binding pocket as erlotinib. Molecular dynamics simulations showed that compounds 3 and 19 formed more stable complexes, maintaining root-mean-square deviation values of approximately 1–3 Å throughout the trajectory, whereas compound 10 displayed greater fluctuations and reduced stability. **Conclusion:** Compounds 3 and 19 exhibited the most favorable combination of binding affinity, dynamic stability, and predicted safety profiles, highlighting their potential as lead candidates for further development as *EGFR* inhibitors in NSCLC.

Keywords: Lung Neoplasms, Carcinoma, Non-Small-Cell Lung, Receptor, Epidermal Growth Factor

Asian Pac J Cancer Prev, **27 (9)**, 3265-3272

Introduction

Non-small cell lung cancer (NSCLC) remains one of the leading causes of cancer-related mortality worldwide, accounting for over 1.8 million new cases and more than 600,000 deaths in 2021 [1]. Its high burden reflects the urgent need for novel therapeutic strategies capable of improving clinical outcomes. Among the molecular drivers of NSCLC, mutations in the epidermal growth factor receptor (*EGFR*) are among the most clinically significant, as they influence tumor progression, apoptosis, and treatment responsiveness. Tyrosine kinase inhibitors (TKIs) such as gefitinib and erlotinib have markedly improved outcomes in *EGFR*-mutant NSCLC [2, 3]. However, despite initial responses, acquired resistance, most notably the T790M substitution, remains a major therapeutic challenge, frequently restoring ATP affinity and diminishing TKI effectiveness [4, 5]. *EGFR* dysregulation continues to promote malignant processes through enhanced motility, cell-cycle disruption, angiogenesis, metastasis, and apoptosis inhibition [6].

Micheliolide (MCL), a guaianolide-type sesquiterpene lactone derived from Michelia compressa and Michelia champaca, has demonstrated anticancer properties through modulation of pathways such as PI3K/Akt and NF-κB and by inducing cell-cycle arrest in several cancer models [7, 8]. The chemical structure of Micheliolide (R = H) is shown in Figure 1. Although MCL and its derivatives exhibit broad anticancer activity, their potential interaction with *EGFR*, particularly within the NSCLC context, has not been explored. No available studies have systematically assessed the drug-likeness, predicted bioactivity, binding characteristics, or dynamic stability of Micheliolide derivatives against *EGFR* [9]. Therefore, this study aimed to identify Micheliolide derivatives previously synthesized by Ma et al. [8], that may demonstrate anticancer potential against NSCLC, with a specific focus on their predicted pharmacokinetic properties and interaction with the *EGFR* kinase domain.

This work is a novel systematic investigation aiming to assess the lack of data regarding Micheliolide derivatives as specific competitive ATP analogs for *EGFR* targeting,

*[1]Department of Internal Medicine, Faculty of Medicine, Universitas Sumatera Utara, Medan, Indonesia. [2]Division of Pulmonology and Critical Care, Department of Internal Medicine, Cipto Mangunkusumo National Hospital – Faculty of Medicine Universitas Indonesia, Jakarta, Indonesia. *For Correspondence: sahathalim@usu.ac.id*

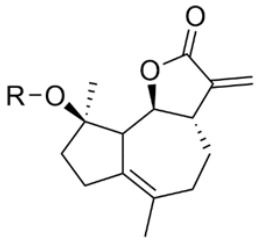

Figure 1. Micheiolide (R = H) Structure

in contrast to previous studies that concentrated on anti-inflammatory and anticancer potential.

Materials and Methods

Study Design

This was an in silico computational study integrating ADMET prediction, bioactivity screening, molecular docking, and molecular dynamics simulations to evaluate the potential of Micheliolide (MCL) derivatives as *EGFR* inhibitors.

Generation of Ligand Structures

Two-dimensional and three-dimensional structures of Micheliolide derivatives were generated using ChemOffice, with ChemDraw employed for 2D construction and Chem3D for 3D structural optimization. All optimized structures were saved in PDB format, and SMILES strings were generated using ChemDraw. Potential bioactivities of each compound were screened using the PASS Online platform due to its extensive training set, especially for cancer-related bioactivities. The *EGFR* protein structure was retrieved from the RCSB Protein Data Bank (https://www.rcsb.org/) in PDB format.

ADME and Toxicity Prediction

Absorption, distribution, metabolism, excretion, and toxicity (ADMET) properties were predicted using SwissADME (http://www.swissadme.ch/) and ADMET-AI (https://admet.ai.greenstonebio.com/) because both complement each other in assessing Lipinski's parameters and quantitative structure-activity relationship (QSAR). SMILES strings for all derivatives were submitted to both platforms, and predicted pharmacokinetic and toxicity profiles were summarized descriptively.

Cancer-Related Bioactivity Screening

Anticancer-related bioactivities were evaluated using the PASS Online tool (http://www.way2drug.com/). Probability of activity (Pa) values were obtained for relevant endpoints, including antineoplastic (lung cancer), general antineoplastic, cytostatic, antimetastatic, anticarcinogenic, chemopreventive, and MMP9-inhibitory properties. Outputs were visualized in a heatmap format.

Molecular Docking

Molecular docking was conducted using AutoDock Vina, with ligand and receptor preparation performed in AutoDockTools 1.5.6. The *EGFR* kinase domain (PDB ID: 1M17) was prepared by removing crystallographic water molecules, adding polar hydrogens, and assigning Kollman charges [10]. Ligands were energy-minimized in Chem3D 23.1.1 using the MM2 force field and converted to PDBQT format. The docking grid was centered on the native ligand (erlotinib) binding site (center_x = 21.697, center_y = 0.303, center_z = 52.093) using a grid box size of 40 × 40 × 40, exhaustiveness of 32, and num_nodes of 20. The lowest binding-energy pose for each compound was selected for visualization in BIOVIA Discovery Studio 2025.

Molecular Dynamics Simulations

Compounds 3, 10, and 19 were selected for molecular dynamics (MD) simulations based on docking affinity and ADMET properties. Protein–ligand complexes were prepared using UCSF Chimera 1.18. MD simulations were performed in GROMACS (CHARMM27 force field) using the SPC water model, with counterion neutralization. Ligand topologies were generated via SwissParam (https://www.swissparam.ch/) [11]. Energy minimization was carried out using 5,000 steps of steepest descent, followed by 100-ps NVT and 100-ps NPT equilibration phases. In order to thermally equilibrate the system while keeping the volume constant, the NVT phase used a V-rescale thermostat set at 300 K. The box volume and solvent density were then allowed to stabilize during an NPT phase using a Berendsen barostat at 1.0 bar. In order to enable a 2-fs integration step, both stages used the LINCS algorithm to constrain H-bonds and Particle Mesh Ewald (PME) for electrostatics. Production simulations were run for 50 ns at 300 K. Root-mean-square deviation (RMSD), root-mean-square fluctuation (RMSF), and radius of gyration (Rg) were extracted and analyzed using Origin 2024.

Statistical Analysis

This study did not involve hypothesis-testing statistical procedures. ADMET predictions, PASS-derived Pa values, docking scores, and MD trajectories were analyzed descriptively. Stability of protein–ligand complexes was assessed using RMSD thresholds (≤3 Å considered stable), RMSF profiles, and Rg patterns. All computational analyses were conducted using AutoDock Vina, GROMACS, Origin 2024, and associated software tools.

Cell Line Authentication

This study did not involve the use of cell lines; therefore, cell line authentication requirements do not apply.

Results

ADME and Toxicity Prediction

All Micheliolide derivatives complied with Lipinski's Rule of Five, indicating favorable physicochemical properties for oral drug candidates. Except for compounds 22 and 23, none of the derivatives possessed hydrogen-bond donor groups. Compounds 10, 11, and 23 exhibited the lowest Quantitative Estimate of Drug-Likeness (QED)

scores.

In the AMES mutagenicity prediction, compound 10 showed the highest probability of mutagenicity, followed by compound 14. Blood brain barrier penetration and CYP1A2 inhibition values were generally similar across all derivatives. Compounds 1 and 3 demonstrated the highest predicted oral bioavailability (Ma model), suggesting strong potential for further development. Table 1 summarizes the Lipinski parameters, drug-likeness scores, and toxicity predictions for all Micheliolide derivatives evaluated in this study.

Cancer-Related Bioactivity Screening

Predicted anticancer bioactivity probabilities for all derivatives are shown in Figure 2. For antineoplastic activity specific to lung cancer, compounds 5, 20, and 14 had the highest Pa values (0.729, 0.727, and 0.727, respectively). For general antineoplastic activity, compounds 14, 16, and 20 ranked highest (Pa = 0.935, 0.933, and 0.916). Compound 20 produced the strongest cytostatic prediction (Pa = 0.780), followed by compounds 5 (0.736) and 14 (0.725).

Regarding antimetastatic potential, compounds 20, 21, and 18 showed the highest predicted probabilities (Pa = 0.515, 0.508, and 0.495). For anticarcinogenic activity, the highest Pa values were seen in compounds 20 (0.239), 21 (0.231), and 1 (0.209). For chemopreventive potential, compound 21 demonstrated the strongest prediction (Pa = 0.382), followed by compounds 20 and 12. Compounds 1 and 2 exhibited the highest predicted MMP9 inhibitory activity (Pa = 0.874 and 0.874), with compound 21 also showing strong activity (Pa = 0.859).

Molecular docking

Molecular docking revealed that most derivatives exhibited stronger predicted binding affinities than the native ligand erlotinib. Docking scores and amino-acid interactions for all Micheliolide derivatives are presented in Table 2. Compound 10 showed the strongest binding affinity (−8.6 kcal/mol), interacting with residues Val702, Ala719, Lys721, and Met742 within the *EGFR* active site.

Compound 19 had the second-highest affinity (−8.0 kcal/mol), forming interactions with Val702, Lys721, Met742, Leu764, and Leu820. Compounds 3, 11, and 20 (all −7.7 kcal/mol) also demonstrated favorable binding, although compound 20 interacted with only a single key residue (Val702), suggesting less stable binding. Figure 3 illustrates the binding-pocket overlap of erlotinib with compounds 3, 10, and 19, confirming that all four ligands occupy the same ATP-binding region of *EGFR*.

Molecular dynamics

Molecular dynamics simulations were performed for compounds 3, 10, and 19 to assess the stability of their *EGFR* complexes (Figure 4). Compound 3 maintained consistent stability throughout the 50-ns trajectory,

Table 1. ADME/ Tox Prediction of Native Ligand and MCL Derivatives

Name	MW (g/mol)	logP	HBA	HBD	TPSA	Lipinski	QED	AMES	BBB-Martins	Bioavailability-Ma	CYP1A2-Veith
Erlotinib	248.32	2.36	3	1	46.53	4	0.41	0.34	0.92	0.78	0.05
1	262.35	3.01	3	0	35.53	4	0.41	0.54	0.96	0.84	0.07
2	338.45	4.58	3	0	35.53	4	0.46	0.49	0.87	0.73	0.2
3	292.38	2.98	4	0	44.76	4	0.35	0.63	0.97	0.84	0.03
4	290.36	2.93	4	0	52.6	4	0.42	0.47	0.95	0.65	0.08
5	304.39	3.32	4	0	52.6	4	0.45	0.4	0.94	0.66	0.09
6	332.44	4.1	4	0	52.6	4	0.44	0.45	0.93	0.61	0.09
7	318.41	3.56	4	0	52.6	4	0.44	0.48	0.91	0.59	0.07
8	332.44	3.95	4	0	52.6	4	0.45	0.52	0.91	0.63	0.04
9	380.48	4.54	4	0	52.6	4	0.44	0.44	0.87	0.67	0.1
10	373.45	4.39	5	0	101.36	4	0.13	0.97	0.91	0.58	0.03
11	330.42	3.87	4	0	52.6	4	0.45	0.51	0.92	0.65	0.11
12	320.39	2.55	5	0	61.83	4	0.45	0.52	0.95	0.69	0.02
13	324.8	3.15	4	0	52.6	4	0.34	0.66	0.93	0.74	0.2
14	359.25	3.71	4	0	52.6	4	0.33	0.77	0.96	0.71	0.19
15	369.26	3.3	4	0	52.6	4	0.32	0.66	0.95	0.69	0.15
16	411.34	4.47	4	0	52.6	4	0.22	0.71	0.96	0.57	0.1
17	302.37	3.09	4	0	52.6	4	0.45	0.47	0.9	0.56	0.15
18	316.4	3.48	4	0	52.6	4	0.44	0.47	0.91	0.59	0.12
19	330.42	3.87	4	0	52.6	4	0.44	0.44	0.9	0.57	0.1
20	378.47	4.62	4	0	52.6	4	0.44	0.44	0.83	0.63	0.2
21	342.44	3.71	4	0	52.6	4	0.26	0.53	0.89	0.54	0.16
22	485.63	4.07	8	1	103.54	4	0.22	0.58	0.8	0.5	0.02
23	248.32	2.36	3	1	46.53	4	0.41	0.34	0.92	0.78	0.05

Abbreviations: MW, molecular weight; HBA, hydrogen bond acceptor; HBD, hydrogen bond donor; TPSA, topological polar surface area; QED, quantitative estimate of drug-likeness; BBB, blood–brain barrier.

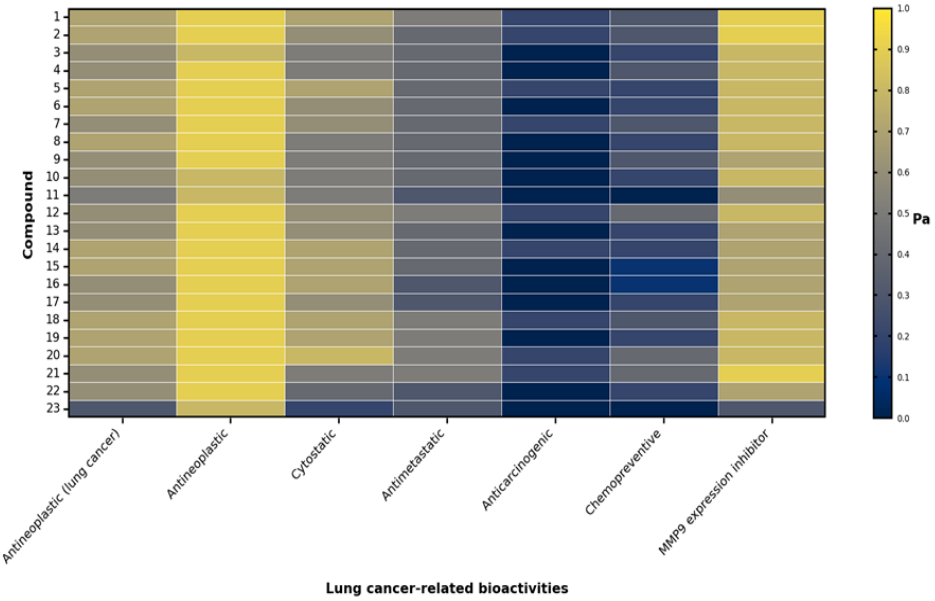

Figure 2. Predicted lung-cancer–related bioactivities of MCL derivatives using PASS Online. Color gradients represent the predicted probability of activity (Pa) for each compound across six bioactivity classes, including antineoplastic (lung cancer), general antineoplastic, cytostatic, antimetastatic, anticancerogenic, chemopreventive, and MMP-expression inhibitory properties. Higher Pa values (yellow) indicate a stronger likelihood of exhibiting the predicted biological effect, while lower Pa values (dark blue) suggest weaker or negligible predicted activity.

with RMSD values remaining below 3 Å. Compound 19 exhibited early fluctuations (2–10 ns), reaching slightly above 4 Å, but stabilized for the remainder of the simulation.

In contrast, compound 10 showed initially stable behavior during the first 5 ns, followed by progressive RMSD increases beyond 3 Å after 30 ns, indicating reduced stability despite its strong docking score. RMSF analysis demonstrated similar residue-level flexibility across all complexes, with a localized increase in fluctuation in residues 962–995 for compounds 3 and 19. Radius of gyration profiles showed minor variability among complexes but no major deviations suggestive of structural destabilization.

Discussion

Lipinski introduced the Rule of Five (Ro5) to guide the development of orally active drug candidates, specifying physicochemical thresholds such as molecular weight below 500 Da, LogP values under 5, and no more than five hydrogen bond donors or ten hydrogen bond acceptors [12]. Lower molecular weight supports membrane permeability [13], while LogP values that are either too high or too low may reduce transport efficiency or alter membrane interactions [14]. All Micheliolide (MCL) derivatives in this study satisfied Ro5 criteria, indicating favorable drug-like characteristics. Most compounds demonstrated QED values ≥0.3, except compounds 10, 11, and 23, suggesting the majority of derivatives possess acceptable drug-likeness [15].

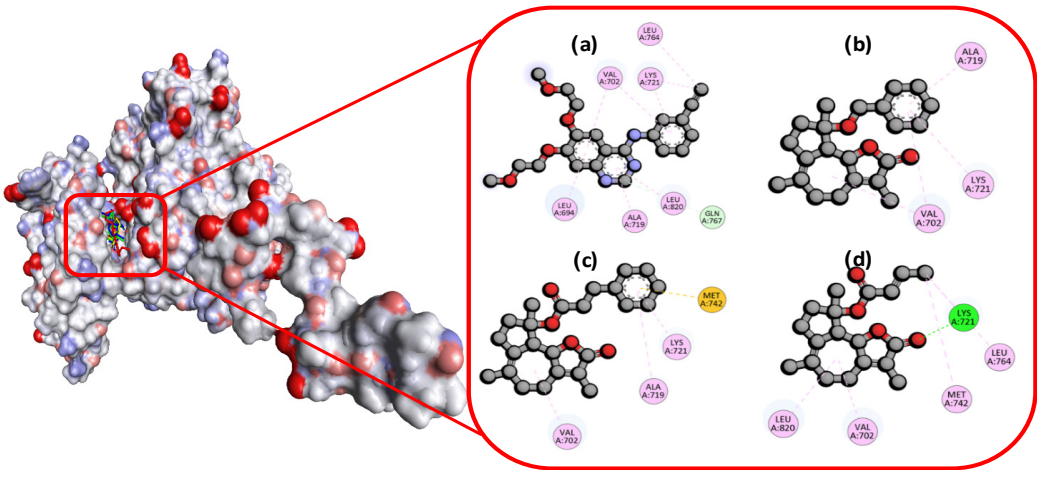

Figure 3. Overlay of Erlotinib (Red), Compound 3 (Green), Compound 10 (Blue), and Compound 19 (Yellow) at the *EGFR* Binding Pocket. Panels show 2D interactions for (a) erlotinib, (b) compound 3, (c) compound 10, and (d) compound 19.

Table 2. Binding Affinity Values and Amino Acid Interactions of MCL Derivatives

Compounds	R	Binding Affinity (kcal/mol)	Amino Acid Interactions
Erlotinib	-	-6.9	Leu694, Val702, Ala719, Lys721, Leu764, Gln767, Leu820
1 (MCL)	-H	-7.3	Val702, Ala719, Gly772, Leu820
2	0	-7.1	Leu694, Val702, Ala719, Gly772, Leu820
3	$-CH_2Ph$	-7.7	Val702, Ala719, Lys721
4	$-CH_2OCH_3$	-7	Val702, Ala719, Gly772, Cys773, Asp776, Leu820
5	$-COCH_3$	-7	Val702, Cys773, Leu820
6	$-COCH_2CH_3$	-7.1	Val702, Cys773, Leu820
7	$-CO(CH_2)_3CH_3$	-6.9	Leu694, Val702, Ala719, Lys721, Leu820
8	$-COCH(CH_3)_2$	-7.4	Val702, Ala719, Cys773, Leu820
9	$-COCH_2CH(CH_3)_2$	-7.6	Val702, Ala719, Lys721, Leu820
10	$-COCH_2CH_2Ph$	-8.6	Val702, Ala719, Lys721, Met742
11	-CO(CH2)4N3	-7.7	Lys721, Leu820
12	$-COCH_2CH_2CHCH_2$	-6.8	Val702, Cys773, Leu820
13	$-COCH_2OCH_3$	-6.9	Val702, Thr766
14	$-COCH_2C_1$	-7.1	Val702
15	$-COCH(C_1)_2$	-7.4	Val702, Gln767
16	$-COCH_2Br$	-6.9	Val702, Cys773, Leu820
17	$-CO(CH_2)_4Br$	-7.3	Leu694, Phe699, Val702, Lys721, Met742, Leu764
18	$-COCH=CH_2$	-7.1	Val702, Cys773, Leu820
19	$-COCH=CHCH_3$	-8	Val702, Lys721, Met742, Leu764, Leu820
20	$-COCH=C(CH_3)_2$	-7.7	Val702
21	-COCH=CHPh	-7.5	Gly695, Phe699, Cys773, Leu820
22	$-CO(CH_2)_3C\equiv CH$	-6.7	Leu694, Val702, Gly772, Cys773, Leu820
23	$-CO(CH_2)_3$-[1-$((CH_2)_6OH)$-1,2,3-triazol-4-yl]	-7.1	Leu694, Phe699, Val702, Ala719, Arg817, Leu820, Asp831

*Highlighted compounds (green) indicate the top-performing candidates selected based on binding affinity and key interactions with *EGFR* active-site residues. Abbreviations: R, substituent on Micheliolide core; binding affinity in kcal/mol; amino acid residues indicate EGFR binding interactions.

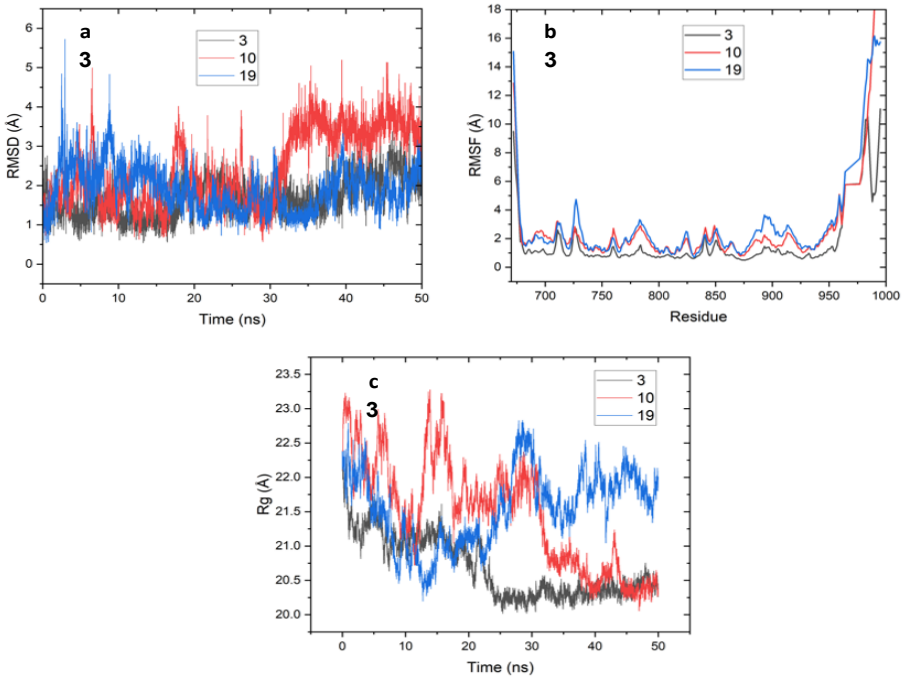

Figure 4. Molecular Dynamics Simulation Profiles of Compounds 3, 10, and 19 in Complex with *EGFR*. (a) Root-mean-square deviation (RMSD) indicating overall complex stability over 50 ns. (b) Root-mean-square fluctuation (RMSF) showing residue-level flexibility across the EGFR backbone. (c) Radius of gyration (Rg) describing the compactness of the protein–ligand complex during simulation. Lower fluctuations in RMSD and Rg reflect greater conformational stability upon ligand binding.

Toxicity predictions further supported compound selection. The AMES mutagenicity model identified compound 10 as having the highest likelihood of mutagenicity, possibly attributable to reactive structural features such as ketone and phenyl groups capable of forming DNA adducts [16, 17]. All compounds showed high predicted blood–brain barrier penetration, although none were intended as CNS-targeted agents. Oral bioavailability estimates revealed compounds 1 and 3 as the most favorable candidates, reinforcing their potential suitability for oral administration [18]. ADMET-AI predictions also indicated generally high intestinal absorption across the series (Figure S1), although compound 11 displayed high predicted toxicity, reducing its priority as a drug candidate. The comparative ADMET profiles of the top-performing compounds (3, 11, and 20) are summarized in Figure S2.

PASS Online bioactivity screening allowed further characterization of pharmacological potential. Most MCL derivatives displayed notable antineoplastic activity specific to lung cancer, whereas only compound 23 showed consistently low activity across multiple anticancer endpoints. Cytostatic activity, representing the inhibition of cell proliferation, was prominent across several derivatives, reflecting potential utility as antiproliferative agents [19, 20]. However, probabilities for antimetastatic activity were relatively low overall, suggesting limited predicted ability to interfere with metastatic processes [21]. MMP9 inhibition, a key component of cancer invasion and metastasis, was strongly predicted for nearly all derivatives except compound 23, consistent with the relevance of MMP9 dysregulation in lung cancer progression [22].

Docking validation produced an RMSD of 1.118 Å (Figure S3), confirming the reliability of the docking protocol. Compounds 3, 10, and 19 exhibited the strongest interactions with *EGFR*, forming contacts with several residues known to mediate erlotinib activity within the ATP-binding site. Erlotinib interacts with residues including Leu694, Val702, Ala719, Lys721, Leu764, Gln767, and Leu820 [23]. Compound 3 reproduced three of these interactions (Val702, Ala719, Lys721), whereas compound 10 formed four interactions, including Met742. Compound 19 recapitulated four erlotinib interactions (Val702, Lys721, Leu764, Leu820) and formed an additional hydrogen bond with Lys721, which likely stabilizes the *EGFR*–ligand complex [24]. These patterns suggest that compounds 3, 10, and 19 may compete with ATP within the active site in a manner similar to erlotinib.

Molecular dynamics simulations provided deeper insight into binding stability. RMSD analysis confirmed that compounds 3 and 19 formed stable complexes, with fluctuations largely within 1–3 Å over the 50-ns trajectory, consistent with stable ligand accommodation [25]. In contrast, compound 10 exhibited rising fluctuations beyond 30 ns, indicating lower dynamic stability despite its strong docking affinity. RMSF results suggested localized flexibility variations upon ligand binding, particularly for compound 19, which induced mobility in residues 726–728 and 892–898. Compactness analyses using radius of gyration (Rg) revealed that complexes with compounds 10 and 19 experienced greater structural variation, whereas the 3-*EGFR* complex maintained a more compact conformation after 25 ns, suggesting stable protein folding during simulation [26].

This study has several limitations. First, all findings were derived from in silico approaches, including ADMET prediction, molecular docking, and molecular dynamics simulations, without experimental validation. Therefore, the biological activity, toxicity, and pharmacokinetic behavior of the identified compounds in real biological systems remain uncertain. Second, although molecular dynamics simulations were performed to assess complex stability, more advanced free energy calculations such as MM-PBSA or MM-GBSA were not conducted, which may provide a more accurate estimation of binding affinity. Third, the simulation duration was limited to 50 ns, which may not fully capture long-term conformational changes of the protein–ligand complex. Finally, the computational models used in ADMET and PASS predictions are based on existing datasets and may not fully represent novel chemical structures. Therefore, further experimental validation, including in vitro and in vivo studies, is required to confirm the therapeutic potential of these compounds.

In conclusion, compounds 3 and 19 demonstrated the strongest overall potential as *EGFR* inhibitors, supported by favorable binding affinity, consistent dynamic stability, low predicted toxicity, and acceptable pharmacokinetic profiles. While compound 10 exhibited the highest docking score, its instability during molecular dynamics reduces its likelihood of serving as a robust inhibitor. The intricacy of the cellular environment and systemic pharmacokinetics in living things cannot be fully explained by molecular docking and dynamics, even though they offer high-resolution insights into possible binding modes. Therefore, further experimental studies will be performed on compounds 3 and 19 as promising leads for further cell viability assays (MTT or CCK-8) in *EGFR*-mutant NSCLC cell lines to determine their IC50 values compared to erlotinib as a positive control.

Author Contribution Statement

SH, D, and CMR conceived and designed the study. SH and AH developed the methodology, with SH responsible for software use, data curation, and project administration. H performed data validation. SH and AH conducted the formal analysis and investigation, while D and CMR provided resources and oversight. SH and AH drafted the original manuscript. SCAN and AMM contributed to critical review and editing. Supervision was provided by D and CMR. All authors reviewed and approved the final manuscript.

Acknowledgements

The authors would like to thank all colleagues and academic mentors who provided scientific input during the development of this study. We also acknowledge the use of publicly available computational tools, including PASS Online, AutoDock Vina, ADMET-AI, and

molecular dynamics simulation resources that supported the completion of this work.

Funding Statement

This research received no external funding. All computational work was conducted using freely accessible or institutionally supported resources.

Ethical Declaration

This study did not involve human participants, animals, or biological specimens. All analyses were performed using publicly accessible data and in silico tools. Therefore, ethical committee approval was not required, and no ethical concerns apply to this research.

Data Availability

All data used in this study were obtained from publicly accessible computational tools and databases. ADMET predictions, docking files, MD trajectories, and processed datasets are available from the corresponding author upon reasonable request.

Study Registration

This study does not require registration, as it is not a clinical trial, clinical guideline, human/animal research, or systematic review involving human data.

Conflict of Interest

The authors declare no conflicts of interest regarding the conduct, interpretation, or publication of this research.

References

1. Siegel RL, Miller KD, Fuchs HE, Jemal A. Cancer Statistics, 2021. CA Cancer J Clin. 2021;71(1):7-33. https://doi.org/10.3322/caac.21654
2. Wu YL, Zhou C, Hu CP, Feng J, Lu S, Huang Y, et al. Afatinib versus cisplatin plus gemcitabine for first-line treatment of Asian patients with advanced non-small-cell lung cancer harbouring *EGFR* mutations (LUX-Lung 6): an open-label, randomised phase 3 trial. Lancet Oncol. 2014;15(2):213-222. https://doi.org/10.1016/S1470-2045(13)70604-1
3. Gervas P, Ivanova A, Vasiliev N, Ananina O, Zharkova O, Rogovieva O, et al. Frequency of *EGFR* mutations in non-small cell lung cancer patients: screening data from West Siberia. Asian Pac J Cancer Prev. 2015;16(2):689-692. https://doi.org/10.7314/APJCP.2015.16.2.689
4. Yu HA, Arcila ME, Rekhtman N, Sima CS, Zakowski MF, Pao W, et al. Analysis of tumor specimens at the time of acquired resistance to *EGFR*-TKI therapy in 155 patients with *EGFR*-mutant lung cancers. Clin Cancer Res. 2013;19(8):2240-2247. https://doi.org/10.1158/1078-0432.CCR-12-2246
5. Gandhi J, Zhang J, Xie Y, Soh J, Shigematsu H, Zhang W, et al. Alterations in genes of the *EGFR* signaling pathway and their relationship to *EGFR* tyrosine kinase inhibitor sensitivity in lung cancer cell lines. PLoS One. 2009;4(2):e4576. https://doi.org/10.1371/journal.pone.0004576
6. Garrido-Castro AC, Felip E. HER2 driven non-small cell lung cancer (NSCLC): potential therapeutic approaches. Transl Lung Cancer Res. 2013;2(2):122-127. https://doi.org/10.3978/j.issn.2218-6751.2013.02.02
7. Vyshnavi H, Namboori K. Identifying potential ligand molecules *EGFR* mediated TNBC targeting the kinase domain-identification of customized drugs through in silico methods. Res Pharm Sci. 2023;18(2):121-137. https://doi.org/10.4103/1735-5362.367792
8. Ma WW, Shi QQ, Ding YH, Long J, Zhang Q, Chen Y. Synthesis of micheliolide derivatives and their activities against AML progenitor cells. Molecules. 2013;18(5):5980-5992. https://doi.org/10.3390/molecules18055980
9. Uddin J, Fatima M, Riaz A, Kamal GM, Bin Muhsinah A, Ahmed AR, Iftikhar R. Pharmacological potential of micheliolide: a focus on anti-inflammatory and anticancer activities. Heliyon. 2024;10(6):e27299. https://doi.org/10.1016/j.heliyon.2024.e27299
10. Sucahyo A, Rahman MF, Khotimah H, Widodo W, Ulfa SM. Identification of flavone and flavanone from ethyl acetate fraction of Caesalpinia sappan heartwood and tentative structure-activity relationship: an in vitro and in silico approach. J Appl Pharm Sci. 2023;13(11):89-100. https://doi.org/10.7324/JAPS.2023.92856
11. Kushwaha PP, Singh AK, Bansal T, Yadav A, Prajapati KS, Shuaib M, Kumar S. Identification of natural inhibitors against SARS-CoV-2 drugable targets using molecular docking, molecular dynamics simulation, and MM-PBSA approach. Front Cell Infect Microbiol. 2021;11:730288. https://doi.org/10.3389/fcimb.2021.730288
12. Protti IF, Rodrigues DR, Fonseca SK, Alves RJ, de Oliveira RB, Maltarollo VG. Do drug-likeness rules apply to oral prodrugs? ChemMedChem. 2021;16(9):1446-1456. https://doi.org/10.1002/cmdc.202000805
13. Varilie N. The influence of molecular size on drug absorption: a comprehensive overview. Ann Clin Trials Vaccines Res. 2024;14(3):242-243. https://doi.org/10.37532/ACTVR.2024.14(3).242-243
14. Lipinski CA. Lead- and drug-like compounds: the rule-of-five revolution. Drug Discov Today Technol. 2004;1(4):337-341. https://doi.org/10.1016/j.ddtec.2004.11.007
15. Bickerton GR, Paolini GV, Besnard J, Muresan S, Hopkins AL. Quantifying the chemical beauty of drugs. Nat Chem. 2012;4(2):90-98. https://doi.org/10.1038/nchem.1243
16. Honma M. An assessment of mutagenicity of chemical substances by (quantitative) structure-activity relationship. Genes Environ. 2020;42:23. https://doi.org/10.1186/s41021-020-00163-1
17. Yun BH, Guo J, Bellamri M, Turesky RJ. DNA adducts: formation, biological effects, and new biospecimens for mass spectrometric measurements in humans. Mass Spectrom Rev. 2020;39(1-2):55-82. https://doi.org/10.1002/mas.21570
18. Price G, Patel DA. Drug Bioavailability. In: StatPearls. Treasure Island (FL): StatPearls Publishing, http://www.ncbi.nlm.nih.gov/books/NBK557852/ (2025, accessed 20 July 2025).
19. Ayon NJ. High-throughput screening of natural product and synthetic molecule libraries for antibacterial drug discovery. Metabolites. 2023;13(5):625. https://doi.org/10.3390/metabo13050625
20. Ratajczak K, Borska S. Cytotoxic and proapoptotic effects of resveratrol in in vitro studies on selected types of gastrointestinal cancers. Molecules. 2021;26(14):4350. https://doi.org/10.3390/molecules26144350
21. Karaman S, Detmar M. Mechanisms of lymphatic metastasis. J Clin Invest. 2014;124(3):922-928. https://doi.org/10.1172/JCI71606
22. Rashid ZA, Bardaweel SK. Novel matrix metalloproteinase-9 (MMP-9) inhibitors in cancer treatment. Int J Mol Sci. 2023;24(15):12133. https://doi.org/10.3390/ijms241512133
23. Stamos J, Sliwkowski MX, Eigenbrot C. Structure of the epidermal growth factor receptor kinase domain alone and in complex with a 4-anilinoquinazoline inhibitor. J Biol

Chem. 2002;277(48):46265-46272. https://doi.org/10.1074/jbc.M207135200
24. Malik FK, Guo J. Insights into protein-DNA interactions from hydrogen bond energy-based comparative protein-ligand analyses. Proteins. 2022;90(6):1303-1314. https://doi.org/10.1002/prot.26313
25. Wargasetia TL, Ratnawati H, Widodo N, Widyananda MH. Bioinformatics study of sea cucumber peptides as antibreast cancer through inhibiting the activity of overexpressed protein (*EGFR*, *PI3K, AKT1*, and *CDK4*). Cancer Inform. 2021;20:11769351211031864. https://doi.org/10.1177/11769351211031864
26. Reza R, Dutta T, Baildya N, Ghosh NN, Khan AA, Das RK. Repurposing of anti-lung cancer drugs as multi-target inhibitors of SARS-CoV-2 proteins: an insight from molecular docking and MD-simulation study. Microb Pathog. 2022;169:105615. https://doi.org/10.1016/j.micpath.2022.105615